

Mesohabitat Spawning Preference of the Anadromous Twaite Shad (*Alosa fallax*, Lacépède 1803) in the Tagliamento River (Italy)

Original

Mesohabitat Spawning Preference of the Anadromous Twaite Shad (*Alosa fallax*, Lacépède 1803) in the Tagliamento River (Italy) / Negro, Giovanni; Lesa, Davide; Bertoli, Marco; Guglielmetto, Alessandro; Pinna, Beatrice; Forte, Simone; Spadavecchia, Claudio; Maschio, Paolo; Pizzul, Elisabetta; Vezza, Paolo. - In: ECOHYDROLOGY. - ISSN 1936-0584. - ELETTRONICO. - 18:1(2025), pp. 1-17. [10.1002/eco.70010]

Availability:

This version is available at: 11583/2998022 since: 2025-03-03T14:55:34Z

Publisher:

Wiley & Sons

Published

DOI:10.1002/eco.70010

Terms of use:




This article is made available under terms and conditions as specified in the corresponding bibliographic description in the repository

Publisher copyright

(Article begins on next page)

RESEARCH ARTICLE OPEN ACCESS

Mesohabitat Spawning Preference of the Anadromous Twaite Shad (*Alosa fallax*, Lacépède 1803) in the Tagliamento River (Italy)

Giovanni Negro¹  | Davide Lesa² | Marco Bertoli³ | Alessandro Guglielmetto¹  | Beatrice Pinna¹ | Simone Forte¹ | Claudio Spadavecchia¹  | Paolo Maschio¹ | Elisabetta Pizzul³ | Paolo Vezza¹

¹Department of Environment, Land and Infrastructure Engineering (DIATI), Polytechnic of Turin, Turin, Italy | ²Ente Tutela Patrimonio Ittico, Udine, Italy | ³Department of Life Sciences, University of Trieste, Trieste, Italy

Correspondence: Giovanni Negro (giovanni.negro@polito.it)

Received: 6 June 2024 | **Revised:** 4 December 2024 | **Accepted:** 16 February 2025

Funding: This work was supported by the Autorità di Bacino Alpi Orientali and the Regione Autonoma Friuli Venezia Giulia.

Keywords: anadromous fish | geomorphic units | habitat suitability criteria | hydrodynamic model | mesohabitat | MesoHABSIM | random forest | spawning habitat preference

ABSTRACT

Alosa fallax (Lacépède, 1803) is an anadromous fish which utilizes European rivers for spawning. As many anadromous species, Twaite shad populations are declining due to river damming and hydromorphological alterations, which impact their spawning sites. In this study, we developed mesohabitat suitability criteria for the spawning period of *A. fallax* by analysing the geomorphic units (GUs), with their local habitat attribute, in which the fish prefers to spawn. The study was conducted in the Tagliamento River (NE Italy). Habitat depiction was performed following the MesoHABitat SIMulation Model (MesoHABSIM) approach. High-resolution spatial information from Uncrewed Aerial Systems (UAS), a two-dimensional (2D) hydrodynamic model and field data collected during the spawning period were utilized for habitat attribute evaluation. The association between spawning sites and GUs characteristics was explored by training a classification random forest (RF) model. The final parsimonious RF model demonstrated high accuracy (98.8%) and true skill statistic (97.6%), indicating that *A. fallax* prefers glides and riffles with shallow depths (0.15–0.45 m), moderate current velocities (0.30–0.75 m/s) and small-sized sediment (diameter 0.2–6 cm) for spawning. Using an infrared camera, 72 surface mating events were distinctly recorded between 11.30 PM and 02.15 AM over two nights, demonstrating the technique's suitability for observing shad mating activity. The video analysis revealed that the monitored *A. fallax* population exhibited similar mating behaviour to other European shads (e.g., *Alosa alosa*). This study provides useful insights to develop novel management approaches for preserving or restoring the spawning habitat of the *A. fallax*, supporting its conservation.

1 | Introduction

Anadromous fish are a particular group of migratory species that exemplify the interlinking of freshwater and marine ecosystems, utilizing both environments to complete their life cycle (Willson, Gende, and Marston 1998). These species are born in freshwater rivers or streams, where, after hatching, they spend the early part of their lives. As they grow, they experience

physiological changes that allow them to migrate downstream and enter the sea. In the marine environments, they spend a significant portion of their lives, before returning to the rivers for breeding (McDowall 2008). Anadromous species provides important ecosystem services (Almeida et al. 2023) and are considered essential contributors to the ecological balance of both fluvial and marine ecosystems, transporting marine-derived nutrients back to freshwater environments and providing a

This is an open access article under the terms of the [Creative Commons Attribution](https://creativecommons.org/licenses/by/4.0/) License, which permits use, distribution and reproduction in any medium, provided the original work is properly cited.

© 2025 The Author(s). *Ecohydrology* published by John Wiley & Sons Ltd.

significant food source for predators in both environments (Willson and Halupka 1995).

However, despite their remarkable adaptability (Schiewe 2013), anadromous fish are facing a multitude of challenges and threats that are undermining their existence. Indeed, among the 16 anadromous species that spawn in the European watercourses, one (*Coregonus oxyrinchus*) is considered extinct, and nine are listed as vulnerable or critically endangered in the IUCN (International Union for Conservation of Nature) Red List (IUCN 2022). Habitat alteration and degradation, overfishing and climate change are considered the most significant factors in the severe decline of these species (Almeida et al. 2023). In particular, river regulation and damming have considerably impacted the streams that serve as breeding and rearing sites for anadromous species. Indeed, river damming determines the fragmentation of the water courses (Seliger and Zeiringer 2018), directly impeding anadromous fish to reach upstream suitable spawning sites. Additionally, dams alter the hydrological regime and impact the supply of sediment and organic material to downstream reaches (Poff et al. 1997; Wohl et al. 2015), crucially influencing the generation of physical breeding habitats for these species. In this regard, recent studies (e.g., Almeida et al. 2023; van Puijenbroek et al. 2019) have pointed out that most efforts to sustain the conservation of anadromous species and the maintenance of their habitat must focus primarily on improving river continuity and preserving and restoring habitat integrity.

To assess the hydromorphological impact related to water abstraction and river regulation, habitat suitability models (HSMs) were conceived (Bovee 1982; Jowett 1997; Parasiewicz 2001). HSMs can be used for a variety of purposes, including river management, environmental flows (e-flows) design, river restoration projects and species conservation plans (Acreman and Dunbar 2004; Parasiewicz, Rogers, et al. 2013; Yi et al. 2017). These tools allow to predict the suitable habitat patches for a target species (or ecological group) by means of habitat suitability criteria (or species' distribution model) developed on its habitat requirements. Species' distribution models usually take into account various environmental parameters such as water depth, flow velocity and substrate composition, which are used to analyse their relationships with the species presence (Ahmadi-Nedushan et al. 2006). Among the different HSMs, the MesoHABSIM (Meso-HABitat SIMulation Model; Parasiewicz 2007) approach is increasingly used, especially in Italy, where it has been established as a reference method for e-flows design (Vezza, Zanin, and Parasiewicz 2017). MesoHABSIM assesses the available habitat for fish or other aquatic organisms by quantifying the suitable mesohabitats. Mesohabitats generally correspond in size and location to geomorphic units (GUs; Belletti et al. 2017), such as pools, riffles, glide and rapids. Mesoscale HSMs consider a wide range of environmental parameters, including water depth, flow velocity, substrate composition, presence of shelters and covers for fish, lateral or longitudinal connectivity of the GU with the main river channel and the GU water surface gradient. This wide range of habitat parameters allows a more effective linking between river hydromorphological features and the distribution of aquatic biota (Vezza et al. 2014, 2015). Furthermore, for large rivers, especially for not wadable conditions, mesoscale HSMs can integrate two-dimensional (2D) hydrodynamic models for

simulating water depth and flow velocity distribution within GUs (Farò et al. 2022, 2023).

In the framework of the MesoHABSIM approach, different statistical techniques, such as decision trees (e.g., Koutrakis et al. 2019), logistic regressions (e.g., Vezza et al. 2012) and machine learning (e.g., Vezza et al. 2014), can be used to develop the habitat suitability criteria. Among the machine learning techniques, random forest (RF; Breiman 2001) algorithm has been successfully applied for identifying the habitat requirements of endangered fish (Vezza et al. 2014), macroinvertebrates (Pinna et al. 2024; Vezza, Ghia, and Fea 2016) and freshwater lampreys (Negro et al. 2023). These applications mainly focused on resident freshwater species (Vezza et al. 2012), whereas less attention was generally given to species which use the river environments only for a specific part of their life cycle, such as anadromous fish.

Among the anadromous species that can be found in the Italian rivers, we focused our attention on the spawning habitat requirements of the Twaite shad (*Alosa fallax*, Lacépède 1803). *A. fallax* belongs to the family of Clupeidae, and its distribution range is quite extensive. It inhabits the Northeastern Atlantic Ocean, ranging from Morocco to Iceland and southern Norway, including the Mediterranean, North and Baltic Seas (Aprahamian, Aprahamian, et al. 2003; Kukuev and Orlov 2018). In Italy, landlocked population is also present in the biggest lakes of Northern part (e.g., Lake Garda, Sabatino, Faria, and Alexandrino 2022). *A. fallax* is considered vulnerable in the Italian IUCN (Rondinini, Battistoni, and Teofili 2022), and it is listed in Annexes II and V of the European Habitats Directive (92/43/EEC) and in Annex III of the Bern Convention. Recent studies on anadromous populations of *A. fallax* have revealed significant genetic differentiation among individuals inhabiting the European shores (Sabatino, Faria, and Alexandrino 2022). Therefore, in this manuscript, we generally refer to *A. fallax* as the shad populating the Mediterranean Sea (Bianco 2002). Several studies investigated the biology of *A. fallax* across European rivers (Aprahamian, Aprahamian, et al. 2003; Bianco 2002; Doherty, O'Maoiléidigh, and McCarthy 2004; López et al. 2011). The adult freshwater phase of *A. fallax* begins with the spawning migration, which typically occurs from February, in the Southern distribution area, to May, in the Northern distribution range. This migration is more pronounced when water temperatures exceed 10°C–12°C (Aprahamian, Baglinière, et al. 2003). Breeding has been documented to occur in both fresh and tidal waters, and mating events typically occurred close to the water surface (López et al. 2011; Magath and Thiel 2013). In freshwater environments, adult shads are able to cover hundreds of kilometres to reach upstream spawning grounds (Manyukas 1989; Quignard and Douchement 1991). The spawning period can last 3–4 months, and the mating activity takes place during night at water temperatures around 18°C–22°C (Aprahamian, Baglinière, et al. 2003).

Although the biology of *A. fallax* has been relatively investigated, few researches focused on the spawning habitat requirements of this species (Negro et al. 2021). Caswell and Aprahamian (2001) reported that, in different rivers of Wales, *A. fallax* prefers to spawn in the fast-flowing shallower areas (<0.45 m) of glide, riffle and runs on different substrate types, from gravel to cobbles (0.2–25.6 cm), whereas deeper pools are used for resting during the day. López et al. (2007, 2011) analysed the spawning habitat used by *A.*

fallax in the Ebro River (Spain). By measuring the depth and velocity in some transects, they reported that the spawning grounds were characterized by fast flow regions (1–1.5 m/s), ranging from 3 to 4 m in water depth above gravel substrate. Similar information is reported in Aprahamian, Baglinière, et al. (2003). They conducted a review of more dated literature sources and argued that Twaite shad spawns in water depths ranging from 0.15 to 9.5 m above various substrates, ranging from mud to cobbles.

With the aim of developing the first mesoscale habitat suitability criteria in literature for the spawning period of *A. fallax*, we carried out different field campaigns in a hydromorphologically homogeneous reach of the Tagliamento River (Northeastern Italy). Habitat depiction was achieved following the MesoHABSIM approach. In particular, high resolution spatial information derived from UAS (Uncrewed Aerial Systems), 2D hydrodynamic simulations and field data were used for the definition and characterization of GUs at the flow conditions available during the spawning period. This information was used to train a classification RF model able to identify the suitable mesohabitat for *A. fallax* to spawn, by analysing the local physical habitat attributes of the GUs within the surveyed subreach. By recording with an infrared camera, the mating activity of the shads along two nights of observation it was further possible to observe and analyse the mating behaviour of such species.

2 | Materials and Methods

2.1 | The Study Area

The Tagliamento River flows from the Alps to the Adriatic Sea for almost 170 km in the Friuli-Venezia Giulia Region (Northeastern Italy), providing a total catchment of about 2850 km². The highest peaks of its basin reach 2700 m, whereas its springs are located near

the Mauria Pass at an elevation of about 1200 m. The Tagliamento watershed mainly belongs to the landscape unit of mountainous areas (Alpine and Pre-Alpine, 85% of total catchment) from its source to the Pinzano section (Figure 1a). Downstream the mountainous areas, riverbanks are not yet confined, and the remaining part is occupied by the plains (15% of total watershed). Its fluvial system is characterized by high coarse sediment supply (Ziliani and Surian 2012), which bestows a wide braided planform pattern, from Socchieve to Madrisio for almost 90 km of the river course. From this section, the river, having dissipated much of its energy, begins to narrow, evolving into a meandering planform before flowing into the sea. An extensive morphological characterization of the water course can be found in Ziliani and Surian (2012, 2016).

The upper part of Tagliamento basin is characterized by an Alpine climate, whereas in the lower reaches, the Mediterranean climate is dominant (Bertoldi et al. 2009). Along its course, the river experiences high seasonal variability in flow, with peak discharges occurring during fall (October–November) and spring (May–June). Conversely, extended periods of flow intermittency, which can also determine the complete disappearance of the water table, may occurs in different portion of the braided reach especially during summer. In the downstream part, from Madrisio to the Adriatic Sea, the river returns to be perennial, due to the water supply provided by the groundwater resurgence phenomenon (Rapti-Caputo and Vaccaro 2009). In the Venzone section, the mean discharge is approximately 90 m³/s, with estimated 2-, 5- and 10-year flood discharges of 1100, 1600, and 2150 m³/s, respectively (Bertoldi et al. 2009). The Tagliamento course is not hindered by any major dam. In the upper part of the basin, water withdrawals are mainly related to hydropower production, whereas few weirs for agricultural purposes are located near Venzone and Pinzano. In the lower part of its course, no river dams or barriers are present, and the stream is free to flow to the sea.

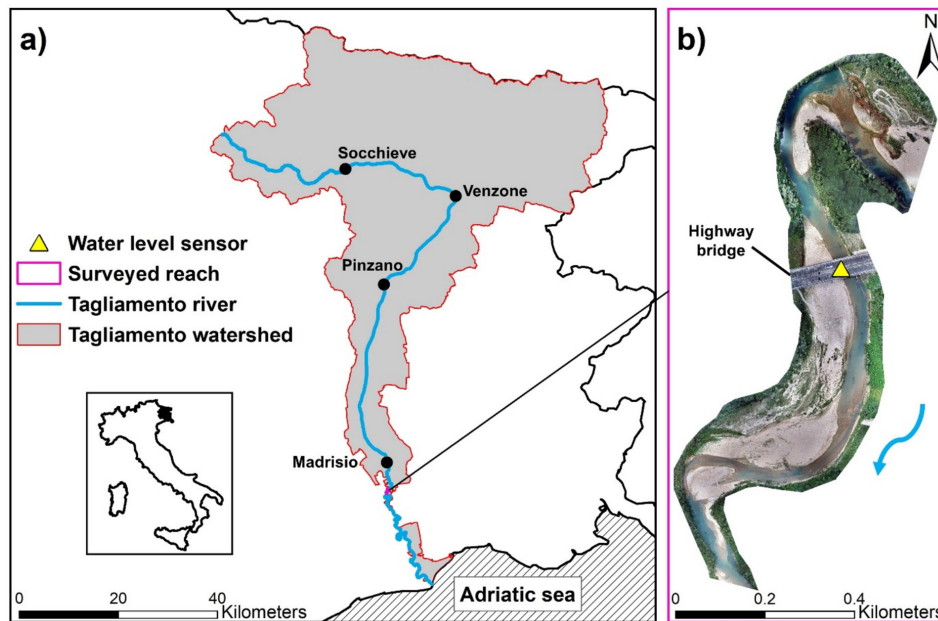


FIGURE 1 | The study area: (a) the Tagliamento watershed and (b) the surveyed subreach, as depicted in the RGB orthomosaic obtained on 1 July 2022. The yellow triangle represents the approximate position of the water level sensor installed in the study site. The primary flow direction is indicated by the blue arrow.

The study site is located in the downstream part of the river (Figure 1), approximately 32km above the estuary in the Adriatic Sea. In this hydromorphologically homogeneous reach, the river planform moves into a transitional morphology characterized by single-thread channels with alternate bars (Gurnell et al. 2014). Surveyed subreach provides a total length of almost 1500 m, and it is characterized by an average width above 100 m. The mean slope is around 0.001, and sediment is mainly composed of small pebbles (2–6 cm), gravel (0.2–2 cm) and sand (<0.2 cm). At the surveyed flow conditions, the GUs' (Belletti et al. 2017) pattern mainly includes (i) glides and riffles with some woody debris, (ii) deep pools (up to 5.5 m) with extensive canopy cover and (iii) few backwaters (Figure 2). Levees and bank protection structures are present to preserve the surrounding settlements and the highway bridge piles, which have directly affected channel morphological dynamics. During the low flow periods, discharge and water temperature does not vary significantly (Figure 3) as mainly contribution to flow is provided by groundwaters (Rapti-Caputo and Vaccaro 2009).

2.2 | Field Surveys and Data Collection

From April 2022 to August 2023, different field campaigns were performed, with the aim of collecting useful data about spawning mesohabitat preferences of *A. fallax* in the surveyed subreach. In particular, it was possible to observe, monitor and analyse the habitat used by the *A. fallax* for mating purposes in two consecutive years.

During the middle of May 2022, a reproduction activity of the shad was detected by the authors within the study site. In order to obtain a river habitat depiction at the mesoscale, the wetted area was broken down into GUs (Belletti et al. 2017), according to the MesoHABSIM approach (Veza, Zanin, and Parasiewicz 2017). Spawning sites were located in particular areas of the surveyed subreach characterized mainly by glides and riffles (Figure 2d). These areas were mapped with a multi-band Real-Time Kinematic Global Navigation Satellite System (RTK GNSS) receiver (Emlid Reach RS2, Emlid, Budapest, Hungary) and registered in a Geographic Information System

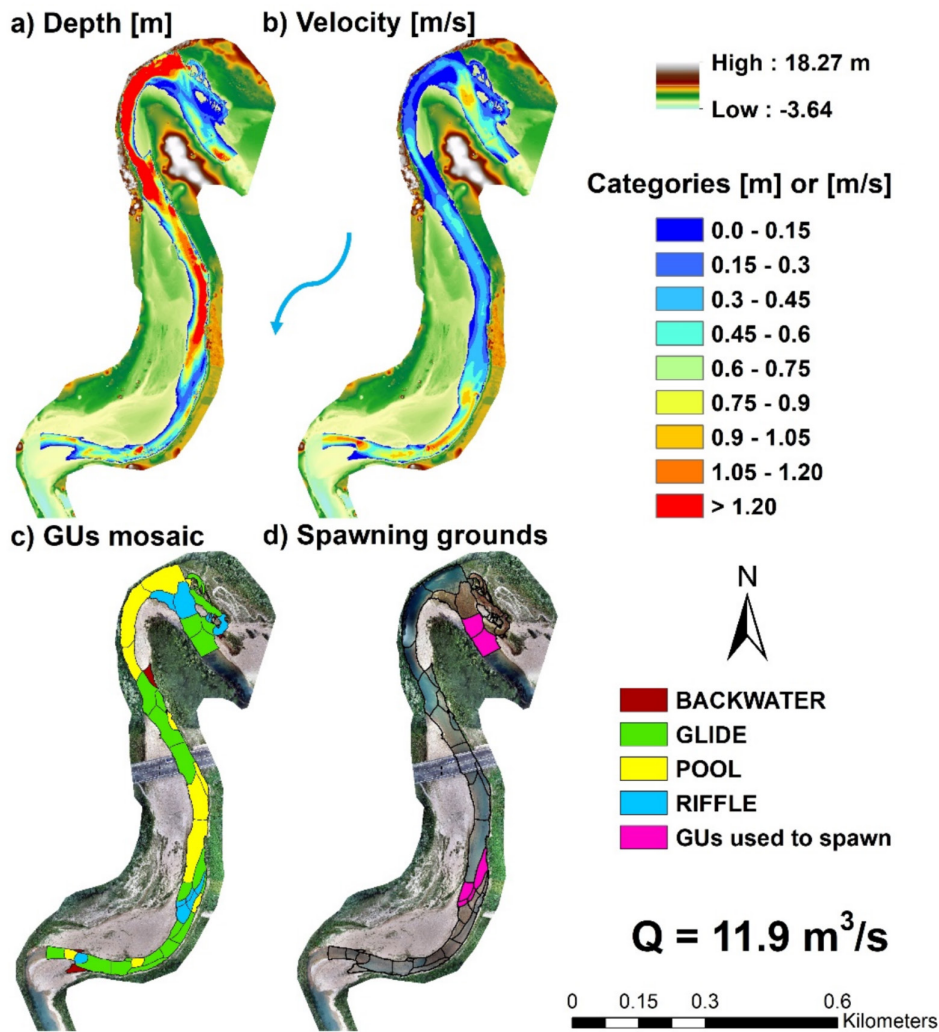


FIGURE 2 | The simulation results for (a) depth and (b) velocity under the flow condition of $11.90 \text{ m}^3/\text{s}$, using the bathymetrically corrected DEM as background. Depth and velocity are colour coded according to the corresponding categories of the MesoHABSIM approach (Table 1), ranging from the smallest (in blue) to the highest (in red). (c) The geomorphic units (GUs) mosaic at flow rate of $11.90 \text{ m}^3/\text{s}$. (d) The GUs where the spawning activities of *A. fallax* were observed are highlighted in purple. The primary flow direction is indicated by the blue arrow.

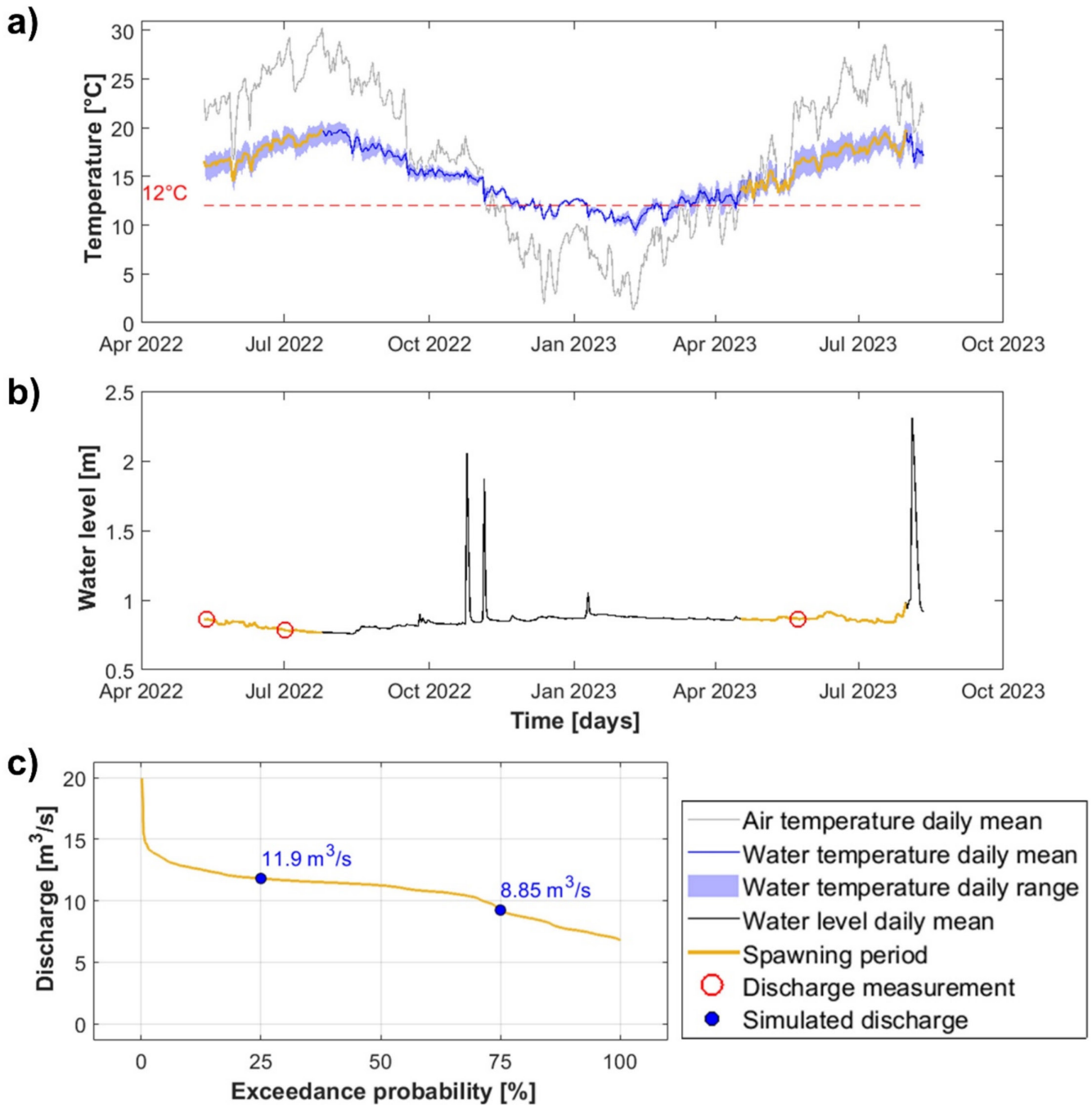


FIGURE 3 | (a) Daily mean air (in grey) and water temperature (in blue) time series from 11 May 2022 to 11 August 2023 registered by the HOBO U20L in the study site. The minimum threshold corresponding to 12°C, above which spawning activities were assumed to start, is represented by a dotted red line. (b) Continuous measurements of the water level (in black) expressed as daily mean values recorded by the sensor installed in the study site. The date in which the discharge measurements were performed during the field campaigns are displayed using red dots. (c) The flow duration curve of the spawning period. The simulated discharges for training the random forest model are highlighted in blue. For all images, the variable corresponding to the spawning period is represented by a continuous orange line.

(GIS) environment. Furthermore, georeferenced information (by means of the RTK-GNSS receiver) about water depth and current velocity were recorded above the spawning sites using the RiverSurveyor M9 Acoustic Doppler Current Profiler (ADCP; Sontek, San Diego, California) installed on a vessel (Williams et al. 2013) and, in the shallower areas, the OTT MF Pro flow metre (Ott HydroMet, Kempten, Germany). Substrate composition was also assessed following the classification of the MesoHABSIM approach (Veza, Zanin, and Parasiewicz 2017).

In particular, individual measuring points were randomly distributed in a stratified manner within the mesohabitats in which spawning was detected. To each measuring point was then assigned the most representative substrate category (Table 1) within the 1 m² area. Thanks to the collaboration with the Ente Tutela Patrimonio Ittico (ETPI), during the surveys, some female specimens of *A. fallax* with eggs were captured using fishing rods. Fish were captured by Dr. Davide Lesa in the deepest pools where they were resting during the daytime. With the

TABLE 1 | The physical habitat attributes used for the geomorphic units (GUs) description in the surveyed subreach. For each habitat parameter, the corresponding categories are expressed as reported in Veza et al. (2014) and Veza, Zanin, and Parasiewicz (2017).

Habitat parameter	Units	Number of categories	Categories/description
Geomorphic units (GUs)	Yes/no	17	Pothole, cascade, rapid, riffle, step, pool, glide, dune, aquatic vegetation, secondary channel, flood lake, wetland, artificial element, waterfall, plunge pool, backwater, rock glide
GU gradient	%	1	Water surface mean gradient of the GU
GU longitudinal connectivity	Yes/no	1	Habitat binary attribute describing mesohabitats longitudinal river connectivity
Depth	Percentage of samples	9	Categories in 0.15 m increments (range 0.0–1.20 m and above)
Velocity	Percentage of samples	9	Categories in 0.15 m/s increments (range 0.0–1.20 m/s and above)
Substrate	Percentage of random samples	12	Gigalithal (rocks), megalithal (> 40 cm), macrolithal (20–40 cm), mesolithal (6–20 cm), microlithal (2–6 cm), akal (gravel > 0.2 cm), psammal (sand), pelal (silt and clay), detritus (organic matter), xylal (woody debris, roots), sapropel (dark anoxic mud), phytal (submerged plants).
Cover	Yes/no	9	Boulders, canopy shading, overhanging vegetation, roots, submerged vegetation, emerging vegetation, undercut banks, woody debris, shallow margins.
Froude number	$(\text{Flow velocity})/(\text{9.81} \cdot \text{depth})^{0.5}$	1	Average over the GU area
Flow velocity standard deviation	cm/s	1	SD over GU area

aim of continuously monitoring flow rate and water temperature in the study site, a water level sensor HOBO U20L (Onset Computer Corporation, Bourne, Massachusetts) was installed in a river cross-section next to the highway bridge (Figure 1). During the survey, river discharge was also measured by means of the RiverSurveyor M9 ($Q = 11.80 \text{ m}^3/\text{s}$).

Two-dimensional numerical models are extensively employed to simulate depth and velocity in rivers for studying in-stream habitat characteristics (e.g., Farò et al. 2023; Jowett and Duncan 2012; Pasternack, Wang, and Merz 2004). In this study, due to the extension of the surveyed subreach, an UAS was used to obtain high resolution topographical information of the river habitat. Aerial images were collected with a DJI Phantom 4 Pro RTK quadcopter (FC6310R Camera Model), with a focal length of 8.8 mm, 5472×3648 pixel resolution and $2.41 \times 2.41 \mu\text{m}$ of pixel size. The flight was performed on 1 July 2022 at an average height of 100 m with a ground sample distance of 1.6 cm/pix, when lower water levels were expected to be in the study site. For validating the spatial information acquired by the UAS, 13 ground control points (GCPs) were placed within the surveyed area, and their position was measured with a Stonex RTK GNSS receiver. The UAS was employed to obtain

both the RGB orthomosaic of the study site (Figure 1b) and the corresponding Digital Elevation Model (DEM; Figure 2a,b), to be used for developing a 2D hydrodynamic model. Concurrent with the flight, a bathymetric survey was carried out by means of the RiverSurveyor M9. In particular, georeferenced information (by means of the RTK-GNSS receiver) about water depth and current velocity were collected by manually displacing the vessel above the water surface, where local depths were above 0.20 m (Muste, Kim, and Merwade 2012). Particular attention was given to the deeper areas (e.g., pools) where the riverbed was less visible from aerial pictures and therefore more difficult for the UAS camera to capture. During the survey, the GUs mosaic was outlined at flow conditions of $Q = 8.15 \text{ m}^3/\text{s}$ and complemented with information about local substrate composition and cover presence.

In May 2023, we confirmed the *A. fallax* presence in the study area, which was again used as a spawning site. During this field campaign, the spawning activity was observed in the same glides and riffles previously mapped, and some females with eggs were caught again by Dr. Davide Lesa in the same pools. After verifying that no significant morphological changes occurred in the surveyed subreach, the data collection operations carried

out in May 2022 were substantially repeated. Discharge was measured equal to $11.90 \text{ m}^3/\text{s}$, which was very close to the condition assessed during the field campaign of May 2022. During this field campaign, with the aim of recording the mating activity of *A. fallax*, we further utilized a GardePro trail camera A3S (GardePro, Hong Kong) equipped with infrared vision to capture videos over the course of two nights. For a nonintrusive monitoring, we strategically positioned the GardePro trail camera on a river bar, in correspondence of the spawning sites downstream the highway bridge (see Figure 2d). By framing the water surface, we continuously recorded from 2330 to 0215 h.

2.3 | Data Analysis and Habitat Description

The 2D images series captured by the UAS sensors were elaborated using the Metashape software (Agisoft, St. Petersburg, Russia), following a common workflow for river applications (e.g., Puig-Mengual et al. 2021; Woodget et al. 2015). In particular, the principles of photogrammetry and the Structure-from-Motion computer vision technique were applied to obtain the RGB orthomosaic (resolution = 1.6 cm) and the 3D model (DEM, resolution = 6 cm) of the surveyed subreach. Although the use of remote optical sensors is widely employed in river science applications (e.g., Dietrich 2017; Lingua et al. 2023), to date, there are no resolute techniques to achieve an automatic reconstruction of the submerged riverbed topography for shallow streams (e.g., Puig-Mengual et al. 2021). The primary challenge in obtaining a precise bathymetric profile of the wetted channel using optical photogrammetric techniques lies in compensating for the light refraction, as it transitions between air and water, which determines an overall overestimation of riverbed elevations (e.g., Tewinkel 1963). However, for shallow and clear water rivers, the relationship between real depth (i.e., really possessed by the riverbed) and apparent ones (i.e., derived from the photogrammetric procedure) can be considered approximately linear, according to the assumptions of the Snell's Law (Veza et al. 2016; Yudha Partama et al. 2017). Therefore, the georeferenced information collected during the bathymetric survey (i.e., 3386 points) was used to train a linear regression model and estimate the real riverbed elevation. This model aimed at capturing the existing linear relationship between the homologous points collected with the RiverSurveyor M9 system (real depth, y) and derived from the photogrammetric processing (apparent depth, x). The resulting bathymetric model ($y = 1.52 * x$, coefficient of determination $R^2 = 0.88$) was then used to reproject the photogrammetric-derived DEM submerged riverbed to the elevations really possessed by the surfaces. For the deeper areas ($> 2 \text{ m}$) where the riverbed was not visible from the UAS sensors, a spatial interpolation was performed directly integrating the georeferenced depth collected by the RiverSurveyor M9. This process was mainly performed in a GIS environment, allowing us to obtain a bathymetrically corrected DEM (Figure 2a,b). To assess the effectiveness of the bathymetric correction applied to the DEM, a validation was then performed. Specifically, considering the same data points employed to train the bathymetric model, the elevations of the bathymetrically corrected DEM were compared with river bottom values acquired by the RiverSurveyor M9, during the bathymetric survey. This analysis was conducted using scatter plots and involved calculating the root mean square errors (RMSE) and the coefficient of determinations (R^2) of the

linear regression model of the first quadrant's bisection (i.e., $y = x$, representing a perfect match between homologous points).

To reconstruct the hydrodynamic conditions of water flow during the spawning period of *A. fallax*, a 2D fixed-bottom numerical model was developed with the HEC-RAS (Hydrologic Engineering Center of U.S.A, Davis, California, Version 5.0.7) software. Following the recommendations of Farò et al. (2023), the mesh construction was built using the DEM bathymetrically corrected of the study area, with a mean grid size of 1 m^2 . For calibrating the hydrodynamic model, we carefully selected the Manning's coefficient (bed roughness), considered constant for the entire study domain (Nicholas 2003), aiming to replicate the local hydraulic conditions measured during the UAS flight. Specifically, we focused on ensuring the best possible agreement between simulated and observed (i.e., derived from the bathymetric survey) depths and velocities, as well as the highest qualitative match between the simulated wetted surface extension and the real one, visible in the RGB orthomosaic. Furthermore, to guarantee model stability and reliability, particular attention was given to the definition of the computational time step, with the aim of maintaining the Courant number below one (Chang and Wang 2002). Once the model was calibrated, we conducted hydrodynamic simulations using the Saint Venant equations under steady-state conditions at 8.85 and $11.90 \text{ m}^3/\text{s}$ (Figure 2). These discharges were chosen as representative of flow conditions commonly encountered by *A. fallax* during their spawning period, as they corresponded to the 75th and 25th percentiles of the flow rate distribution recorded by the water level sensor (Figure 3). Furthermore, the flow of $8.85 \text{ m}^3/\text{s}$ did not deviate much from the hydraulic conditions during the UAS flight ($Q = 8.15 \text{ m}^3/\text{s}$), which were used for calibrating the hydrodynamic model. The $11.90 \text{ m}^3/\text{s}$ discharge, meanwhile, substantially overlapped the discharges recorded in both the field campaigns of May 2022 and 2023, when direct observations on the mesohabitat used by *A. fallax* to spawn were performed. This latter simulated discharge allowed a further validation of the hydrodynamic model by comparing the georeferenced water depths and velocity values recorded above the spawning sites using the RiverSurveyor M9 and the OTT MF Pro flow metre (i.e., 1009 points) with the homologous simulated values.

The output of the hydrodynamic simulations was exported in raster format and used synergically with the DEM and the RGB orthomosaic for the identification and definition of the GUs mosaic at the simulated flow conditions, according to what was recorded during the field campaigns. The mesohabitats representation was achieved using a GIS environment, storing the information in polygon shapefiles. As required by the MesoHABSIM approach, each GUs must be described with several habitat parameters (Table 1). Depth and velocity distributions were assessed by extracting them from the output of the hydrodynamic simulations. Substrate composition, GUs longitudinal connectivity and cover presence was derived from the georeferenced information collected during the field surveys, which were integrated and validated by referring to the RGB orthomosaic. Finally, GUs gradient was defined using the spatial information of both the DEM and the simulated water depths.

The data recorded by the HOB0 U20L permitted to obtain water level and temperature time series of the study site, spanning

from May 2022 to August 2023 (i.e., 15 months; Figure 3). These locally acquired series were used to infer the spawning period for *A. fallax*. Water temperature is recognized to significantly influence the spawning activity of freshwater fish (Pankhurst and Munday 2011); therefore, we mainly focused on this variable for framing the reproduction period. According to Aprahamian, Baglinière, et al. (2003), we set a minimum daily temperature threshold (12°C) above which spawning activities were assumed to commence (Figure 3a). Reproduction was considered to persist until the mean water temperature trend continued to increase, that is, before reaching the annual maximum value. In this way, the end of the spawning period approximately coincided with the end of July for both 2022 and 2023 (lasting 3–4 months; Aprahamian, Baglinière, et al. 2003). Over these periods, water levels, and consequently discharges, do not vary significantly (Figure 3b). The discharge measurements from the field surveys allowed us to establish the correlation between water levels registered by the sensor (Figure 3b) and the evolution of stream flows throughout the entire spawning period. Specifically, we transformed the water level series into a water surface elevation (WSE) series, derived from the hydrodynamic model, assuming a linear relationship between these variables. The linear regression model was trained using both the water levels recorded by the sensor and the simulated WSEs corresponding to all available discharge measurements (i.e., 8.15, 11.80, and 11.90 m³/s). Consequently, the flow rating curve (Figure S1) was determined by interpolating WSE values derived from nine simulations conducted in the range of 6.00 to 20.00 m³/s through a third-degree polynomial function, with coefficients determined using the least-squares method (e.g., Fenton 2018; Herschy 2008). The resulting flow duration curve for the spawning period is illustrated in Figure 3c, providing a basis for defining the typical discharge conditions under which *A. fallax* was assumed to spawn. Specifically, two flow conditions were considered—8.85 m³/s (Q75) and 11.90 m³/s (Q25)—for which hydrodynamic simulations were performed.

Finally, the videos captured during two nights in May 2023 were analysed in order to (i) confirm the mesohabitat selection by *A. fallax* for spawning, (ii) better understand the mating behaviour of *A. fallax* and (iii) quantify the occurrence of surface mating episodes from the video records. Considering this latter aspect, particular attention was placed on distinguishing between actual mating events and mere mating attempts. In our video analysis, a successful spawning event was defined as an instance where the fish rapidly circled each other for a minimum of 3 s.

2.4 | Mesohabitat Suitability Criteria

Probabilistic models were utilized to investigate the spawning habitat preferences of *A. fallax* by examining the association of GUs characteristics with the breeding areas used for mating activity within the surveyed subreach. To identify the mesohabitat attributes (Table 1) preferred by *A. fallax* for spawning, the random forest (RF) classification algorithm, introduced by Breiman (2001), was employed.

This ensemble machine learning technique has found wide use in ecology due to its numerous advantages in effectively addressing classification problems. RF ability to handle

high-dimensional datasets in a time-effective manner, to model intricate interactions among predictor variables and reduce overfitting makes it particularly well suited for ecological applications (Cutler et al. 2007). In particular, RF has been quite leveraged for shaping the habitat suitability criteria of different aquatic organism in the framework of the MesoHABSIM approach (Negro et al. 2023; Pinna et al. 2024; Vezza et al. 2014; Vezza, Ghia, and Fea 2016).

RF, as implemented in R (library randomForest, Version 4.6-7, Liaw and Wiener 2002), relies on aggregating a large set of randomized trees, which are trained by selecting a random learning sample, achieved through bootstrap sampling (Breiman 1996), from the original dataset. To construct each branch of the trees, a binary recursive partitioning technique is exploited, based on a random selection of a predictor from the variable space. The value of the predictor that determines each partitioning is established in order to minimize the Gini impurity, thereby maximizing class imbalance in the resulting nodes. This process continues until a specified minimum number of observations in the terminal nodes is reached. The out-of-bag (OOB) data are the elements not included in the bootstrap sample, which, by majority voting, allows for cross-validated accuracy estimates across all trees.

For distinguishing between the unsuitable and suitable mesohabitat for the spawning of the shad, we developed a binary classification model involving two Boolean responsive classes (defined as 0/1), where 1 indicated a > 50% predicted probability of being a suitable GU for spawning. Both simulated flow conditions (8.85 and 11.90 m³/s) were included in the analysis to ensure that the criteria could capture a broader range of habitat attributes, reflecting the typical spawning period conditions for *A. fallax* within the surveyed subreach. By considering all GUs described in the surveyed subreach at the two simulated flow conditions, the prevalence (i.e., frequency of mesohabitats in which the breeding activity was observed) was found to be 11.5%. Consequently, with the aim of obtaining a balance database, we implemented and tested a model that involved a prior random oversampling of the training dataset. In particular, we used the Synthetic Minority Over-sampling Technique (SMOTE; Chawla et al. 2002), which facilitates the oversampling of the minority class by introducing synthetic instances along the line segments connecting all the *k*-minority class nearest neighbours.

Our primary focus was on obtaining the final parsimonious model with the highest predictive performance. To achieve this, we conducted rigorous predictors selection and fine-tuned the hyperparameters. In particular, to assess the importance of each predictor, we utilized the Boruta algorithm, a popular wrapper for feature selection in the context of RF modelling (Kursa and Rudnicki 2010). Based on the Boruta analysis, we could select the most important predictors, and, to avoid redundancy, we checked for high correlation (Spearman's rho correlation coefficient > 0.8) between them. Among these predictors, a further analysis for selecting the smallest number of variables that provided the best possible classification results was performed, as an excessive number of predictors could lead to increase the OOB error (Kohavi and John 1997). Twelve variables were finally selected for the parsimonious RF model (Figure 4). Concerning hyperparameters tuning, we directed our attention towards those that are known

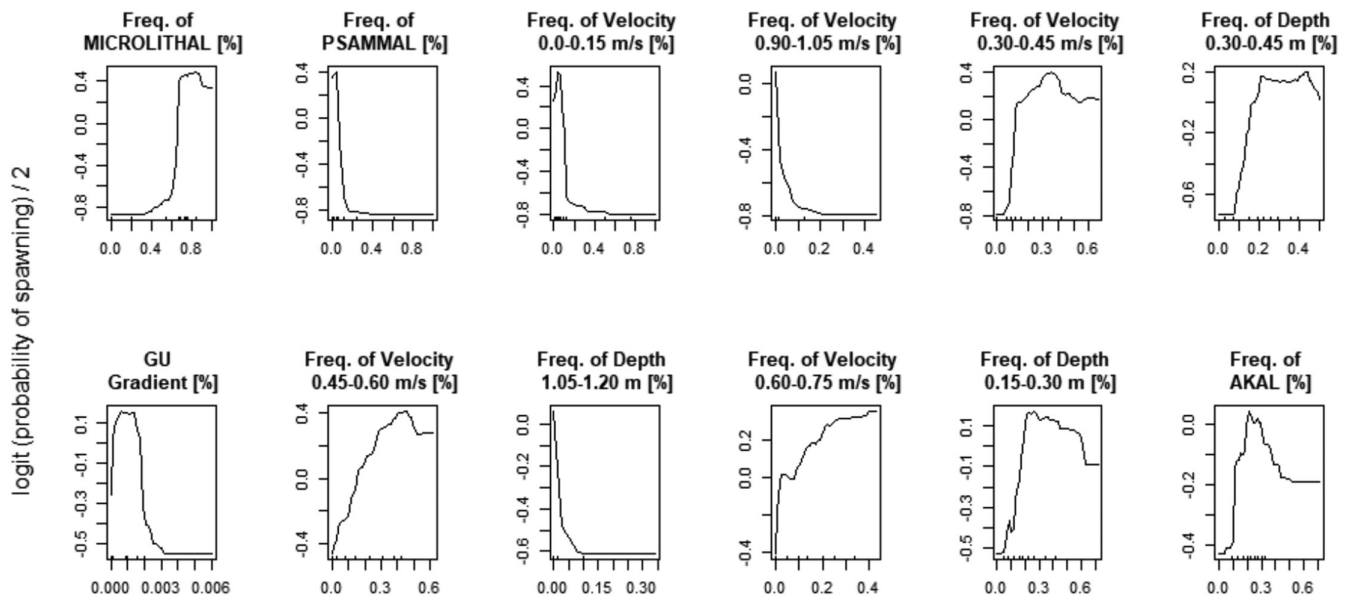


FIGURE 4 | The random forest model for the spawning period of *A. fallax*. The selected physical habitat attributes (Table 1) for the SMOTE parsimonious model are presented in order of importance, ranked by the application of the Boruta algorithm, through partial dependence plots, which express the relationship between attributes and the probability of presence.

to have substantial impact on enhancing model accuracy (Probst, Wright, and Boulesteix 2018). Specifically, we focused on (i) the number of decision trees (*ntree*) and (ii) the number of predictors randomly sampled at each node (*mtry*). The *ntree* value was evaluated equal to 1000, following the recommendation of Evans and Cushman (2009), whereas the *mtry* parameter was established equal to 3 and computed as the square root of the total number of selected predictors included in the model, following the approach of Probst, Wright, and Boulesteix (2018). To assess the predictive performance of the RF model, we used accuracy, sensitivity, specificity and the true skill statistic (TSS), proposed by Allouche, Tsoar, and Kadmon (2006). Finally, we employed partial dependence plots (PDPs), which provided valuable insights into the model's interpretability, allowing to visualize the marginal effect of the selected variables on the spawning habitat preferred by *A. fallax* (Cutler et al. 2007).

3 | Results

The validation of the bathymetrically corrected DEM achieved a RMSE of 0.12 m and an R^2 value of 0.92; therefore, it was considered suitable to be employed as topographic information for the hydrodynamic model. For calibrating the 2D hydrodynamic model, the highest match between simulated and observed water depths and velocities was obtained for a Manning's coefficient equal to 0.03. In particular, for water depth, we achieved a RMSE equal to 0.13 m ($R^2=0.93$), whereas flow velocity showed lower performance (RMSE=0.14 m/s and $R^2=0.83$). Generally, the highest errors for depth were localized in correspondence of the deepest areas (>1.50 m), where acquiring river bottom data was more challenging for the UAS sensors. For velocity, we observed that the hydrodynamic model slightly underestimating the highest values (>0.90 m/s). Considering the hydrodynamic model validation at 11.90 m³/s, we generally observed a satisfactory match between the observed and simulated

depths (RMSE=0.05 m; Scatter Index=0.11) and velocities (RMSE=0.14 m/s; Scatter Index=0.22).

In the surveyed subreach, it was possible to identify 104 GUs, 52 GUs for each simulated flow condition (Figure 2c). The highest amount of GUs (45.2%) corresponded to glides, followed by pools (21.1%) and riffles (20.2%). The remaining GUs consisted of backwaters, accounting for 13.5% of cases. Water surface area of the identified GUs varied from a minimum of 5.5 m², which correspond to a backwater, to a maximum of 4889.6 m², which corresponded to a pool. Mean water depth for the flow rate 8.85 m³/s was 0.85 m, whereas mean water depth for the flow rate 11.90 m³/s was 0.88 m. Mean flow velocities were estimated to 0.33 and 0.38 m/s at the flow rates 8.85 and 11.90 m³/s, respectively. The riverbed substrate in glides and riffles was mainly constituted by microlithal (41.1% of total sampled points) and akal (22.9% of total sampled points). Psammal and pelal were mostly identified as the dominant substrate within pools and backwaters, corresponding to the 26.6% and 4.6% of total sampled points, respectively. Regarding fish covers, woody debris was the most common shelter for fish (observed in 68 GUs), followed by shallow margins (observed in 59 GUs). Canopy shading and boulders were observed in 32 and 16 GUs, respectively. Longitudinal and lateral connectivity was observed for all GUs, and GUs' water surface gradient ranged between 0 and 0.008.

Within the study site, all observed mating events of *A. fallax* occurred at night and were limited to specific areas of the surveyed subreach. These areas were located just upstream of notable increases in riverbed slope, typically between pools and subsequent riffles. Under the simulated flow condition of 11.90 m³/s, these areas corresponded to six GUs identified as glides or riffles (Figure 2d). These GUs were also assumed to be suitable at the simulated flow condition of 8.85 m³/s, as direct field observations at this lower flow rate were not feasible. This

assumption was made after assessing a high degree of consistency in the distribution of depth, velocity and substrate values between both simulated flow conditions. Indeed, when considering the MesoHABSIM categories (see Table 1), the p value of the Kolmogorov–Smirnov test was higher than 0.95 for all three variables. Consequently, the total number of GUs deemed suitable for spawning was 12, with an overall prevalence of 11.5%. Of these, eight GUs were classified as glides, and four were identified as riffles. These mesohabitats were characterized by medium water depth (0.15–0.75 m), moderate to high current velocity (0.15–0.9 m/s) and a substrate composition of microlithal and akal with minimal sandy patches. Woody debris (present in 100% of suitable GUs) and shallow margins (found in 66.7% of suitable GUs) were the most common cover features within these areas. During the daytime, however, *A. fallax* spent most of their time in adjacent deep pools presumably for resting, characterized by high water depths (up to 5.5 m), very low flow velocities (close to zero), fine sediment compositions (primarily psammal and pelal), extensive canopy cover and the presence of boulders.

The water level sensor enabled the assessment of water temperature evolution in the study site over 15 months of monitoring (from May 2022 to August 2023; Figure 3a). Absolutely, the minimum water temperature (8.6°C) was recorded at the beginning of February 2023, whereas the maximum temperature (21°C) occurred in late July 2023. The spawning period extended from 11 May (the commencement of records) to 25 July 2022, whereas for 2023, it was longer, ranging from 16 April to 31 July. Among the two considered periods, air and water temperature varied over the ranges 7.8°C–35.4°C (mean value = 22.6°C) and 12.1°C–21°C (mean value = 17.0°C), respectively.

Considering water levels, three significant peaks corresponding to high discharges can be clearly identified in the series (Figure 3b). The highest value occurred on 14 August 2023

(2.31 m), with the subsequent two occurring on 25 October (2.06 m) and 5 November (1.87 m) 2022. Minimum water levels were recorded in mid-August 2022, bottoming values of 0.76 m. Focusing on the spawning period, water levels do not varied significantly, ranging between 0.77 and 0.98 m (mean value = 0.84 m). Specifically, for 2022, maximum values were recorded at the beginning of the series, reflecting a decreasing trend in the water level series during this season. In contrast, for 2023, water levels were more variable, with periods of higher and lower values, depending on the occurrence of rainy events and the corresponding flow rates. The flow rating curve was computed using nine data points (i.e., WSEs derived from hydrodynamic simulations) and exhibited a good capability to approximate the data (RMSE = 0.11 m³/s; R^2 = 0.99, Figure S1). In this way, we evaluated the flow rates during the spawning period that spanned from 6.00 to 20.00 m³/s (mean value = 10.71 m³/s), reflecting the same trend described for the water level series (Figure 3c).

During the field campaign of May 2023, mean water temperature was $16.4 \pm 1^\circ\text{C}$, mean air temperature was $21.7 \pm 3^\circ\text{C}$ and the moon was waxing crescent. The nonintrusive method we employed proved effective for monitoring *A. fallax* spawning behaviour, successfully capturing 72 mating events and 35 mating attempts over two nights (Figure 5). This approach allowed for precise localization of each event within the mesohabitats of the surveyed subreach. Spawning activity was slightly higher on the first night, accounting for 61% of the total events, and tapered slightly on the second. Peak mating activity for both nights occurred between 0030 and 0130 h, representing more than 50% of the total observed events. Mating episodes were generally brief, lasting from 3 to 11 s (mean = 5.5 s). Nearly 80% of these events involved a single mating pair, though in the remaining instances, up to four fish were distinguished participating simultaneously, with these group events typically lasting longer (> 6 s). Mating events were usually solitary, although we

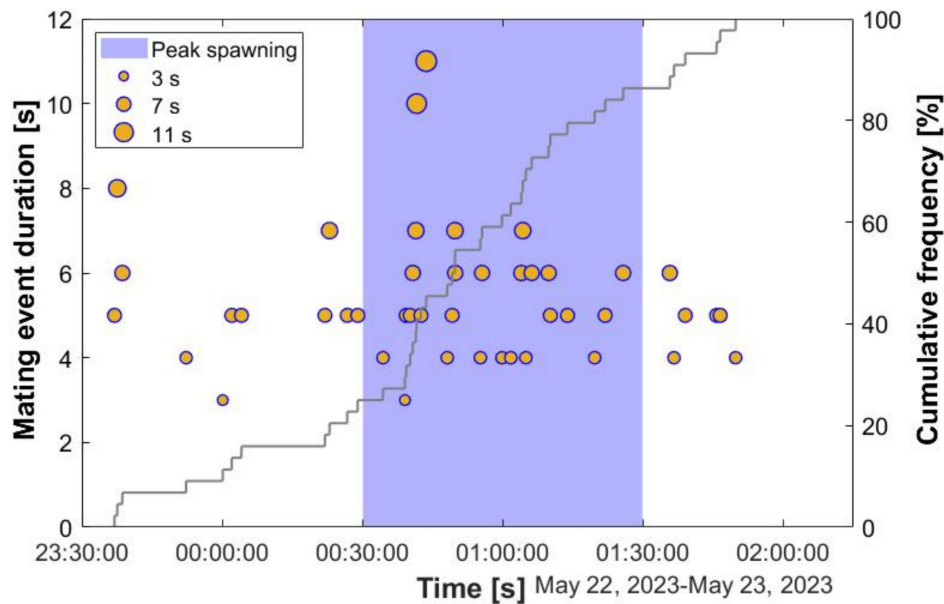


FIGURE 5 | Occurrence (orange dot) and duration (dot size) of mating events recorded by the infrared camera during the first night of observation of the field campaign of May 2023. The broken line in grey represents the cumulative frequency of total mating events (44) recorded during the observation period. The assessed peak spawning time is highlighted in blue.

observed one instance where two mating episodes occurred almost simultaneously in close proximity (Figure 5). Fish showed a slight preference for clockwise rotation during mating (55% of cases). Events were often preceded by pre-mating surface activity, consistently occurring upstream in the area used immediately later for spawning. Other features of mating activity recorded with the camera included (i) fast movements for engaging interactions and (ii) tail splashing, which is a common behaviour of *A. fallax* during spawning (Aprahamian, Baglinière, et al. 2003; López et al. 2011).

The implemented RF models allowed the identification of the most important physical habitat attributes for *A. fallax* spawning, leading to the definition of the first habitat suitability criteria in the literature for this species. The SMOTE parsimonious RF model demonstrated superior predictive performance, emerging as the final selected model (Figure 4). Through cross-validation, this model achieved an overall accuracy of 98.8%, a sensitivity (true positive rate) of 100%, a specificity (true negative rate) of 97.6% and a TSS of 97.6%. The final RF model incorporated 12 mesohabitat attributes, as depicted in Figure 4 through PDPs and ranked according to their importance. Overall, substrates emerged as the most important predictors. Specifically, microlithal (2–6 cm) resulted positively correlated with suitable mesohabitats for spawning, whereas psammal (sand) was negatively correlated. Considering velocities, both low (0.0–0.15 m/s) and high (0.90–1.05 m/s) values provided a negative influence on shad mating habitat selection. In contrast, favoured categories (0.30–0.45; 0.45–0.60; and 0.60–0.75 m/s) corresponded to medium velocities. Similarly, the probability of being a suitable GUs for spawning increased with the presence of medium depths (categories = 0.15–0.30 and 0.30–0.45 m) and decreased with the presence of high values (category = 1.05–1.20 m). Finally, low GU gradients (<0.002) and a presence of akal (gravel) from 20% to 40% positively influenced the shad GU selection for spawning.

4 | Discussion

Anadromous fish species of Italian rivers are facing a multitude of challenges that increasingly threaten their survival (Almeida et al. 2023). Yet detailed knowledge on their ecological requirements, particularly those related to spawning habitat preferences, remains limited (Negro et al. 2021). This study takes an important first step in addressing this gap by examining the meso-habitat preferences and reproductive behaviour of an *A. fallax* population that spawns in the lower reaches of the Tagliamento River (Northeastern Italy).

Within the study site, the spawning activities of *A. fallax* were exclusively observed in glides and riffles. These findings align with those reported in Caswell and Aprahamian (2001) for shad populations in Welsh rivers, where the same types of GUs were observed to be used for mating purposes. Another comparable behaviour observed in shads corresponds to the utilization of deep pools during the daytime, where fish likely rest and gather before moving to the spawning sites during night (Aprahamian, Baglinière, et al. 2003; Caswell and Aprahamian 2001). Thus, the presence of deep pools in close proximity to suitable spawning sites can provide shelters for *A. fallax* during daytime and may constitute an important environmental feature.

To gain a clearer understanding of the habitat preferences, we applied the RF classification algorithm, which enhanced our ability to discern correlations between *A. fallax* spawning requirements and mesohabitat attributes incorporated in the MesoHABSIM approach. Specifically, the final parsimonious RF model, composed of 12 habitat attributes, revealed that for mating purposes *A. fallax* typically looked for glides or riffles distinguished by medium depth (0.15–0.45 m), moderate current velocity (0.30–0.75 m/s) and a small-sized substrate (microlithal and akal). These habitat features align closely with those reported in prior studies on Welsh and French rivers (Caswell and Aprahamian 2001; Quignard and Douchement 1991), suggesting shared ecological preferences across regions. Focusing on substrates, Caswell and Aprahamian (2001) reported that shads also spawned over coarser substrates (cobble, 6.4–25.6 cm). However, such sediment was almost absent in the study site (less than 1% of the total amount). Conversely, López et al. (2011) documented mating activities on gravel substrates in the Ebro River (Spain). Nevertheless, they reported the use of higher values of depths and velocities for spawning: 3–4 m for depth and 1–1.5 m/s for velocity. Together, these findings suggest that *A. fallax* may exhibit a certain flexibility in substrate and hydraulic preferences, being able to adapt to local hydromorphological conditions at specific spawning sites.

The RF algorithm already proved its effectiveness in identifying the habitat requirements for freshwater species in the framework of the MesoHABSIM approach (Negro et al. 2022, 2023; Vezza et al. 2014; Vezza, Ghia, and Fea 2016). The high predictive performance (Accuracy = 98.8%; TSS = 97.6%) achieved for current application reaffirms its capabilities. Consequently, this methodology can be considered appropriate for identifying suitable GUs for the spawning of anadromous species. Nevertheless, to evaluate the transferability of the proposed habitat suitability criteria to other rivers, we are planning a future validation campaign to test the RF model in other rivers and spawning sites. This effort will help validate the criteria across diverse environments and further refine our understanding of *A. fallax* meso-scale habitat requirements.

Reproductive modes among freshwater fish exhibit remarkable diversity, encompassing variations in partner selection, spawning sites and periods and distinct strategies for parental care (Wootton and Smith 2014). Particularly, defining the spawning period can be challenging due to variations influenced by different environmental factors, which commonly are not monitored (i.e., local water temperature). Given the limitations of performing frequent river surveys, in this study, we attempted to indirectly determine the spawning period of *A. fallax* using temperature time series locally recorded. This variable is considered to exert a high level of influence on the spawning period for anadromous fish (Pankhurst and Munday 2011). Indeed, in a recent study that aimed at predicting the occurrence of spawning in *Alosa alosa*, a species closely related to *A. fallax*, using machine learning algorithms and considering various environmental factors, one of the most significant predictors was found to be precisely temperature (Paumier et al. 2020). Despite the importance of this information, the monitoring of discharge within the Italian river network is limited to a restricted number of stream gauges, mainly located along major water courses. Moreover, there is an almost complete absence of gauging

stations measuring water temperatures. In the context of climate change, where extreme events (both floods and droughts) are on the rise, and temperatures are increasing, having this source of information can be crucial for the preservation of anadromous species like *A. fallax*. Therefore, mayor attention should be directed towards the installation of monitoring stations for both discharge and temperatures in rivers.

To establish the commencement of the spawning period, we defined 12°C as the minimum water temperature threshold, above which spawning was considered to begin. This value was taken as reference after consulting the available literature (e.g., Aprahamian, Aprahamian, et al. 2003). However, a higher degree of uncertainty surrounded the upper thermal limit we selected, as direct confirmation in the field was not possible to be achieved. In this case, we considered that the spawning period lasted until the day in which the maximum annual water temperature is reached. This choice was based on (i) literature, which reports a suitable water temperature range of 18°C–22°C and a reproduction period lasting 3–4 months (Aprahamian, Baglinière, et al. 2003), (ii) an overall low fluctuation in water levels over the corresponding amount of time and (iii) information provided by local fishermen on the presence of *A. fallax* in the study site. Compared to the findings reported by Aprahamian, Baglinière, et al. (2003) and López et al. (2007) in the literature, the spawning events we documented in May 2023 took place at a marginally lower water temperature, fluctuating between 14.6°C and 17.8°C. This variation could be linked to the particular hydrological characteristics of the study site, where, during periods of low flow, groundwater significantly contributes to the overall flow. Indeed, the maximum water temperature recorded in the dataset (21°C) is comparatively low for rivers at the latitude of the surveyed subreach (e.g., Vigiak et al. 2017). Additionally, the diel variation in water temperature during the monitored period generally showed minimal fluctuations (< 3°C). The relatively stable thermal regime observed in our data suggests only minor thermal differences between individual mesohabitats, especially at night. Thus, water temperature appears not to play a fundamental role in spawning habitat selection by shads at the mesohabitat scale within the surveyed subreach, indicating that this environmental feature may exert a stronger influence at a higher spatial scale (i.e., reach scale). However, the relevance of thermal variability within mesohabitats could vary depending on river morphology. As observed by Tonolla et al. (2010) in a more morphologically complex, upstream braided reach of the Tagliamento River, thermal differences among mesohabitats might be more pronounced and could potentially influence spawning behaviour. Investigating such morphology-dependent thermal variability would offer valuable insights into whether mesohabitat-level temperature variations play a role in spawning site selection, particularly in braided or multithread reaches.

Water level series allowed the definition of the flow evolution during the spawning period of shads. For its definition, we calibrated a flow rating curve by means of a consolidated approach successfully employed for large rivers (Qader Mirza 2003). Due to the scope of the research, the flow duration curve (Figure S1) was exclusively defined for the spawning period. During the monitored period, the flow varied between 6.00 and 20.00 m³/s, and the lowest discharges were assessed in summer 2022. This

reflects the important drought period, which affected Northern Italy along this year (Bonaldo et al. 2023). Consequently, a slightly general underestimation of the flow range, which typically characterized the spawning period of shad in the study site, may be occurred.

Monitoring the spawning activity of *A. fallax* poses significant challenges due to the complexity of obtaining detailed information on mating behaviour in the water column and precisely locating spawning grounds at night. Traditional methods, such as electrofishing, are typically unsuitable for assessing the species distribution of nocturnal fish spawners, as they are intrusive and not recommended for nighttime use. Acoustic records, which rely on direct hearing to locate and count mating events by capturing sounds produced during reproduction, have been a common alternative (e.g., López et al. 2011). However, these data collection strategies often struggle to precisely locate mating events and typically require multiple observers distributed along the river reach, making them labour intensive and prone to human error. In this study, we explored a novel, nonintrusive approach using cost-effective infrared cameras mounted on tripods along the riverbanks near spawning sites. This technique represents a significant advancement in monitoring *A. fallax* spawning activity, as it allows for continuous and comprehensive visualization of mating events, thereby facilitating a more accurate assessment of both the behaviour of individuals involved and the spatial distribution of these events (Figure 6). The use of infrared cameras enabled the simultaneous monitoring of a substantial river area (10¹–10³ m²), comparable to the extent of GUs (Belletti et al. 2017), providing a feasible solution for assessing the mesohabitats utilized by shads for spawning. This capability offers significant advantages in studies aimed at understanding the habitat requirements of nocturnal surface fish spawners at the mesoscale. Indeed, as demonstrated in this study, employing such equipment allows for the precise localization of mating events, thereby identifying the GUs used to spawn. Additionally, this approach requires minimal human intervention, reducing the number of operators needed and enabling cost-effective monitoring. The ease of use of commercial infrared cameras further enhances the practicality of this method. To address potential limitations related to spatial resolution, particularly in complex riverine environments, future research could explore the integration of infrared cameras with UAS. Such integration could extend coverage area and improve spatial resolution, making the technique even more effective for applications within the MesoHABSIM framework.

Concerning the mating behaviour observed through the analysis of the videos, we noted a close resemblance to descriptions provided by previous researchers studying various shad populations in Europe. This similarity might be linked to the level of genetic differentiations identified in multiple samples of *A. fallax* populations by (Sabatino, Faria, and Alexandrino 2022). These findings indeed suggest a certain level of interactions and potential interchange among populations residing in different regions of the distribution area. In particular, the peak spawning activity took place between 0030 and 0130h, a timeframe that aligns with information reported in the literature. Aprahamian, Baglinière, et al. (2003) mentioned, in their

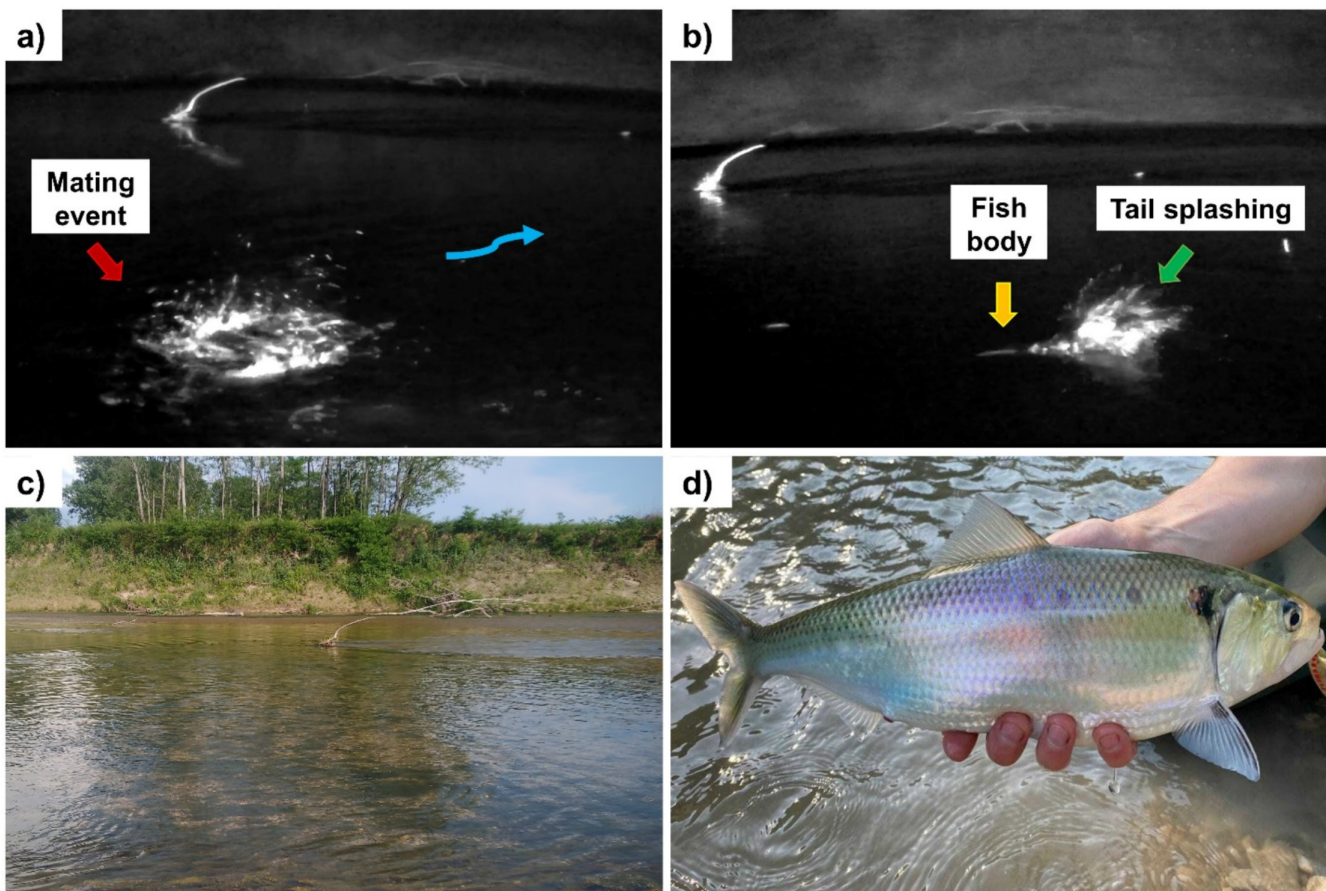


FIGURE 6 | Video frames and pictures recorded during the field campaign in May 2023 with infrared and optical cameras. (a) Example of successful mating event recorded by the infrared camera. The primary flow direction is indicated by the blue arrow. (b) A pre-mating activity (tail splashing). (c) A daily vision of the analysed spawning sites. (d) A specimen of *A. fallax* captured by Dr. Davide Lesa within a deep pool closed to the spawning site.

review, a peak in mating activity occurring between 2200 and 0300 h. More recently, López et al. (2011) observed a peak time at 0215 h in the Ebro River, whereas Langkau et al. (2016) noted the maximum mating activity between 0100 and 0130 h for *A. alosa* in the Garonne River (France). The duration of mating events we evaluated also corresponded with the findings of previous authors (Aprahamian, Baglinière, et al. 2003; López et al. 2011). However, possibly due to the more accurate recording technique we used, we generally observed a slightly longer duration, ranging from 3 to 11 s. Interestingly, we observed that the longest mating events typically involved a higher number of individuals (up to four fish). Nocturnal spawning is an adaptive strategy to minimize exposure to predators (Šmejkal et al. 2018). Consequently, we speculated that moon phases might influence the mating activity of *A. fallax*, anticipating a higher activity during the new moon when lower light conditions prevail. Our hypothesis found some support in our observations, as we noted a declining trend in the number of mating events during the two nights of recording under a waxing crescent moon. Interestingly, Langkau et al. (2016) reported an increasing trend in mating activity for *A. alosa* during three nights of observation under a waning crescent moon. However, it is surprising that we could not find additional confirmation of a potential correlation between *A. fallax* mating events and moon phases in the literature. This aspect necessitates further investigations to better understand the environmental factors that may influence the

reproduction of *A. fallax* also at higher spatial scale (i.e., catchment scale). Lastly, we analysed the prevalent sense of rotation exhibited by fish during mating events in an attempt to identify any potential preference. We found no significant preferred direction of rotation, as both clockwise and counterclockwise rotations were utilized in nearly equal proportions. However, there was a slight prevalence of clockwise rotation, accounting for 55% of the total visible mating events, compared to counterclockwise rotations. Surprisingly, we did not find any existing literature discussing this aspect.

The integrations of acoustic devices and optical remote sensing systems for measuring river hydromorphological dynamics are increasingly used to describe and model river systems (Muste, Kim, and Merwade 2012). These methods are particularly gaining prominence for depicting physical habitat at the mesoscale in shallow water gravel-bed rivers, especially when conducting in-stream surveys proves challenging (Farò et al. 2023; Parasiewicz, Ryan, et al. 2013; Pasternack 2011). For such applications, one of the main objectives is generally the reconstruction of the riverbed topography at an elevated spatial resolution. However, a significant constraint in photogrammetric-derived 3D models consisted in a systematic overestimation of submerged riverbed elevation due to light refraction at the air-water interface. In this study, we used spatially distributed georeferenced depths, collected through a bathymetric survey, for correcting the

submerged riverbed derived from the UAS data processing. This correction was achieved through an empirical approach based on the training of a locally calibrated monoparametric linear regression model. The high data fitting between corrected and measured elevations ($RMSE=0.12$; $R^2=0.92$) aligns with the results obtained by Yudha Partama et al. (2017). In particular, they showed that this method generally proves more effective in reprojecting the apparent depths into real values compared to other approaches based exclusively on the Snell's law. Furthermore, if bathymetric data are available, it is generally easier to be implemented compared to other approaches, which performed the correction using trigonometric functions (e.g., Dietrich 2017) or sophisticated deep learning algorithms (e.g., Agrafiotis et al. 2019).

Bathymetric data collected using Doppler-based devices represent a fundamental source of information for calibrating a hydrodynamic model. In this study, to fine-tune model parameters (e.g., bed roughness), we chose a spatially distributed approach (i.e., 3386 points), harnessing the advantages of employing a moving vessel as a data collector. Compared to transect-based procedures, this approach is considered superior in capturing the spatial heterogeneity in hydraulic features, allowing to achieve a higher level of agreement between model predictions and in-stream measurements (Williams et al. 2013). The high degree of correspondence between simulated and observed data over the spawning sites can be attributable precisely to the use of this distributed approach. In line with common occurrences in hydrodynamic models (e.g., Williams et al. 2013), our model absolutely better predicted depth rather than velocity values. This can be mainly related to the high spatial and temporal variability of velocities recorded through in-stream measurements. Indeed, flow velocity variation is generally influenced by multiple factors such as local channel geometry, bed roughness, potential presence of aquatic vegetation and woody debris.

River habitat evaluation was accomplished using the MesoHABSIM approach, integrating data from various field campaigns and the results of 2D hydrodynamic simulations to describe the GUs. Specifically, georeferenced data obtained from in-stream surveys, along with high spatial resolution information, enabled to obtain a detailed representation of the riverine habitat of the study site. Nonetheless, the flow conditions analysed for defining the habitat suitability criteria closely resembled those observed during the data collection campaigns, facilitating a more accurate convergence and validation between observed and simulated conditions.

5 | Conclusions and Remarks

Spawning habitat requirements for Italian freshwater fish are not sufficiently investigated. Negro et al. (2021) found only 11 studies dedicated to quantitatively describe spawning habitat preferences. With the aim of preserving freshwater fish biodiversity, our analysis revealed that *A. fallax* primarily utilizes glides and riffles as spawning grounds. These areas are characterized by shallow depths (0.15–0.45 m), moderate current velocities (0.30–0.75 m/s) and small-sized substrate, notably microlithal (2–6 cm) and akal (gravel).

The study's methodology, which integrates high-resolution field data with machine learning techniques, proved effective in identifying critical habitat requirements within the MesoHABSIM framework. Indeed, the developed RF model exhibited high predictive performances (Accuracy=98.8% and TSS=97.6%). Therefore, the proposed approach demonstrated strong potential for assessing available habitat for anadromous species in rivers, providing a valuable tool for the conservation and enhancement of their spawning habitats.

In addition, this study employed a novel, nonintrusive approach using cost-effective infrared cameras to capture detailed information on the spawning behaviour of *A. fallax*. This technique allows for continuous, comprehensive visualization of spawning events, supporting accurate assessments of individual behaviour and spatial event distribution. The successful use of infrared technology to monitor mating activity marks a significant advancement in observing nocturnal surface-spawning fish species, establishing a noninvasive methodology that can be adapted for similar studies on other fish populations.

Given the knowledge gaps highlighted by this study regarding the ecological needs of *A. fallax* during its breeding season, further research is urgently needed, particularly in Italy, where no monitoring framework currently exists to assess spawning sites and population status for this species. In this context, the findings from this study provide an important tool for identifying and assessing potential spawning sites within Italian rivers. However, effective conservation of *A. fallax* requires a multiscale approach. Beyond preventing local habitat alterations, broader river and basin-scale measures are essential, encompassing upstream and downstream sections of reproductive habitats. The maintenance of suitable GUs for reproduction requires not only an adequate flow regime and sediment supply but also an adequate degree of river connectivity, enabling *A. fallax* to access spawning sites during its ascent from the sea.

Finally, preserving the quality of spawning habitats will require active monitoring of water quality and temperature, especially during the breeding season, to prevent degradation and maintain optimal conditions for *A. fallax* reproduction. Through these measures, this study aims to contribute foundational data for *A. fallax* conservation while advancing techniques and criteria for effective habitat assessment and species management.

Author Contributions

All authors have made a substantial, direct and intellectual contribution to the work and approved it for publication.

Acknowledgements

This research was supported by the Autorità di Bacino Alpi Orientali and the Friuli-Venezia Giulia Region. We extend our gratitude to the Ente Tutela Patrimonio Ittico (ETPI) of the Friuli-Venezia Giulia Region for their valuable assistance in identifying the spawning site of *Alosa fallax* in the Tagliamento River. We also thank Dr. Alessandro Candiotti, Dr. Paolo Lo Conte and Prof. Francesco Nonnis Marzano for their support during the analysis of the video.

Conflicts of Interest

The authors declare no conflicts of interest.

Data Availability Statement

The data that support the findings of this study are available from the corresponding author upon reasonable request.

References

- Acreman, M., and M. J. Dunbar. 2004. "Defining Environmental River Flow Requirements—A Review." *Hydrology and Earth System Sciences* 8, no. 5: 861–876. <https://doi.org/10.5194/hess-8-861-2004>.
- Agrafiotis, P., D. Skarlatos, A. Georgopoulos, and K. Karantzalos. 2019. "DepthLearn: Learning to Correct the Refraction on Point Clouds Derived From Aerial Imagery for Accurate Dense Shallow Water Bathymetry Based on SVMs-Fusion With LiDAR Point Clouds." *Remote Sensing* 11, no. 19: 2225. <https://doi.org/10.3390/rs11192225>.
- Ahmadi-Nedushan, B., A. St-Hilaire, M. Bérubé, É. Robichaud, N. Thiémonge, and B. Bobée. 2006. "A Review of Statistical Methods for the Evaluation of Aquatic Habitat Suitability for Instream Flow Assessment." *River Research and Applications* 22, no. 5: 503–523. <https://doi.org/10.1002/rra.918>.
- Allouche, O., A. Tsoar, and R. Kadmon. 2006. "Assessing the Accuracy of Species Distribution Models: Prevalence, Kappa and the True Skill Statistic (TSS)." *Journal of Applied Ecology* 43, no. 6: 1223–1232. <https://doi.org/10.1111/j.1365-2664.2006.01214.x>.
- Almeida, P. R., C. S. Mateus, C. M. Alexandre, et al. 2023. "The Decline of the Ecosystem Services Generated by Anadromous Fish in the Iberian Peninsula." *Hydrobiologia* 850, no. 12–13: 2927–2961. <https://doi.org/10.1007/s10750-023-05179-6>.
- Aprahamian M. W., C. D. Aprahamian, J. L. Bagliniere, R. Sabatie, and P. Alexandrino. 2003. "Alosa alosa and Alosa fallax spp. Literature Review and Bibliography."
- Aprahamian, M. W., J. L. Baglinière, M. R. Sabatié, P. Alexandrino, R. Thiel, and C. D. Aprahamian. 2003. "Biology, Status, and Conservation of the Anadromous Atlantic Twaite Shad Alosa Fallax Fallax." *American Fisheries Society Symposium* 35: 103–124.
- Belletti, B., M. Rinaldi, M. Bussettini, et al. 2017. "Characterising Physical Habitats and Fluvial Hydromorphology: A New System for the Survey and Classification of River Geomorphic Units." *Geomorphology* 283: 143–157. <https://doi.org/10.1016/j.geomorph.2017.01.032>.
- Bertoldi, W., A. Gurnell, N. Surian, et al. 2009. "Understanding Reference Processes: Linkages Between River Flows, Sediment Dynamics and Vegetated Landforms Along the Tagliamento River, Italy." *River Research and Applications* 25, no. 5: 501–516.
- Bianco, P. G. 2002. "The Status of the Twaite Shad, Alosa Agone, in Italy and the Western Balkans." *Marine Ecology* 23, no. SUPPL. 1: 51–64. <https://doi.org/10.1111/j.1439-0485.2002.tb00007.x>.
- Bonaldo, D., D. Bellafiore, C. Ferrarin, et al. 2023. "The Summer 2022 Drought: A Taste of Future Climate for the Po Valley (Italy)?" *Regional Environmental Change* 23, no. 1: 1–6. <https://doi.org/10.1007/s10113-022-02004-z>.
- Bovee, K. D. 1982. *A Guide to Stream Habitat Analysis Using the Instream Incremental Flow Methodology*. Instream Flow Information Paper. United States Fish and Wildlife Service FWS/OBS-82/26 (Vol. 12, Issue 82).
- Breiman, L. 1996. "Bagging Predictors." *Machine Learning* 24, no. 2: 123–140. <https://doi.org/10.1007/BF00058655> /METRICS.
- Breiman, L. 2001. "Random Forests." *Machine Learning* 45, no. 1: 5–32. <https://doi.org/10.1023/A:1010933404324>.
- Caswell, P. A., and M. W. Aprahamian. 2001. "Use of River Habitat Survey to Determine the Spawning Habitat Characteristics of Twaite Shad (*Alosa fallax* Fallax)." *BFPP - Bulletin Francais de La Peche et de La Protection des Milieux Aquatiques* 362–363: 919–929. <https://doi.org/10.1051/kmae:2001027>.
- Chang, S., and X. Wang. 2002. "Courant Number Insensitive CE/SE Euler Scheme." 38th AIAA/ASME/SAE/ASEE Joint Propulsion Conference & Exhibit. <https://doi.org/10.2514/6.2002-3890>.
- Chawla, N. V., K. W. Bowyer, L. O. Hall, and W. P. Kegelmeyer. 2002. "SMOTE: Synthetic Minority Over-Sampling Technique." *Journal of Artificial Intelligence Research* 16: 321–357. <https://doi.org/10.1613/JAIR.953>.
- Cutler, D. R., T. C. Edwards, K. H. Beard, et al. 2007. "Random Forests for Classification in Ecology." *Ecology* 88, no. 11: 2783–2792. <https://doi.org/10.1890/07-0539.1>.
- Dietrich, J. T. 2017. "Bathymetric Structure-From-Motion: Extracting Shallow Stream Bathymetry From Multi-View Stereo Photogrammetry." *Earth Surface Processes and Landforms* 42, no. 2: 355–364. <https://doi.org/10.1002/esp.4060>.
- Doherty, D., N. O'Maoiléidigh, and T. K. McCarthy. 2004. "The Biology, Ecology and Future Conservation of Twaite Shad (*Alosa fallax* Lacépède), allis Shad (*Alosa alosa* L.) and Killarney Shad (*Alosa fallax* Killarneyensis Tate Regan) in Ireland." *Biology and Environment: Proceedings of the Royal Irish Academy* 104, no. 3: 93–102. <https://doi.org/10.3318/BIOE.2004.104.3.93>.
- Evans, J. S., and S. A. Cushman. 2009. "Gradient Modeling of Conifer Species Using Random Forests." *Landscape Ecology* 24, no. 5: 673–683. <https://doi.org/10.1007/s10980-009-9341-0>.
- Farò, D., K. Baumgartner, P. Vezza, and G. Zolezzi. 2022. "A Novel Unsupervised Method for Assessing Mesoscale River Habitat Structure and Suitability From 2D Hydraulic Models in Gravel-Bed Rivers." *Ecohydrology* 15, no. 7: 1–18. <https://doi.org/10.1002/eco.2452>.
- Farò, D., K. Baumgartner, P. Vezza, and G. Zolezzi. 2023. "Sensitivity of Fish Habitat Suitability to Multi-Resolution Hydraulic Modeling and Field-Based Description of Meso-Scale River Habitats." *Journal of Hydrology X* 21: 100160. <https://doi.org/10.1016/j.hydroa.2023.100160>.
- Fenton, J. D. 2018. "On the Generation of Stream Rating Curves." *Journal of Hydrology* 564: 748–757. <https://doi.org/10.1016/j.jhydrol.2018.07.025>.
- Gurnell, M., M. Bussettini, B. Camenen, M. González Del Tánago, R. Grabowski, D. Hendriks, A. Henshaw, A. Latapie, and M. Rinaldi (2014). REStoring Rivers FOR Effective Catchment Management (REFORM). Deliverable D2.1 Part I. A Hierarchical Multi-Scale Framework and Indicators of Hydromorphological Processes and Forms.
- Hersch, R. W. 2008. "Streamflow Measurement: Third Edition." 1–507.
- IUCN. 2022. "IUCN Red List of Threatened Species." <https://www.iucnredlist.org/>.
- Jowett, I. G. 1997. "Instream Flow Methods: A Comparison of Approaches." *Regulated Rivers: Research and Management* 13, no. 2: 115–127. [https://doi.org/10.1002/\(SICI\)1099-1646\(199703\)13:2<115::AID-RRR440>3.0.CO;2-6](https://doi.org/10.1002/(SICI)1099-1646(199703)13:2<115::AID-RRR440>3.0.CO;2-6).
- Jowett, I. G., and M. J. Duncan. 2012. "Effectiveness of 1D and 2D Hydraulic Models for Instream Habitat Analysis in a Braided River." *Ecological Engineering* 48: 92–100. <https://doi.org/10.1016/j.ecoleng.2011.06.036>.
- Kohavi, R., and G. H. John. 1997. "Wrappers for Feature Subset Selection." *Artificial Intelligence* 97, no. 1–2: 273–324. [https://doi.org/10.1016/S0004-3702\(97\)00043-X](https://doi.org/10.1016/S0004-3702(97)00043-X).
- Koutrakis, E. T., S. Triantafyllidis, A. S. Sapounidis, et al. 2019. "Evaluation of Ecological Flows in Highly Regulated Rivers Using the Mesohabitat Approach: A Case Study on the Nestos River, N. Greece." *Ecohydrology and Hydrobiology* 19, no. 4: 598–609. <https://doi.org/10.1016/j.ecohyd.2018.01.002>.
- Kukuev, E. I., and A. M. Orlov. 2018. "New Subspecies of Twaite Shad Alosa Fallax Balticus (Clupeidae)." *Inland Water Biology* 11, no. 4: 407–416. <https://doi.org/10.1134/S1995082918040119>.

- Kursa, M. B., and W. R. Rudnicki. 2010. "Feature Selection With the Boruta Package." *Journal of Statistical Software* 36, no. 11: 1–13. <https://doi.org/10.18637/jss.v036.i11>.
- Langkau, M. C., D. Clavé, M. B. Schmidt, and J. Borcherding. 2016. "Spawning Behaviour of Allis Shad *Alosa alosa*: New Insights Based on Imaging Sonar Data." *Journal of Fish Biology* 88, no. 6: 2263–2274. <https://doi.org/10.1111/jfb.12978>.
- Liaw, A., and M. Wiener. 2002. "Classification and Regression by randomForest." *R News* 2, no. 3: 18–22. <https://journal.r-project.org/articles/RN-2002-022/RN-2002-022.pdf>.
- Lingua, A. M., P. Maschio, A. Spadaro, P. Vezza, and G. Negro. 2023. "Iterative Refraction-Correction Method on MVS-SfM for Shallow Stream Bathymetry." *International Archives of the Photogrammetry, Remote Sensing and Spatial Information Sciences* 48, no. 1/W1–2023: 249–255. <https://doi.org/10.5194/ISPRS-ARCHIVES-XLVIII-1-W1-2023-249-2023>.
- López, M. A., K. B. André, R. Sánchez, et al. 2011. "First Characterization of the Spawning Habitat and Mating Behaviour of Twaite Shad in the Ebro River (Western Mediterranean)." *Journal of Applied Ichthyology* 27, no. SUPPL. 3: 53–55. <https://doi.org/10.1111/j.1439-0426.2011.01852.x>.
- López, M. A., N. Gázquez, J. M. Olmo-Vidal, M. W. Aprahamian, and E. Gisbert. 2007. "The Presence of Anadromous Twaite Shad (*Alosa fallax*) in the Ebro River (Western Mediterranean, Spain): An indicator of the population's Recovery?" *Journal of Applied Ichthyology* 23, no. 2: 163–166. <https://doi.org/10.1111/j.1439-0426.2006.00797.x>.
- Magath, V., and R. Thiel. 2013. "Stock Recovery, Spawning Period and Spawning Area Expansion of the Twaite Shad *Alosa fallax* in the Elbe Estuary, Southern North Sea." *Endangered Species Research* 20, no. 2: 109–119. <https://doi.org/10.3354/esr00490>.
- Manyukas, Y. L. 1989. "Biology of the Atlantic Shad, *Alosa fallax* Fallax." *Journal of Ichthyology* 29: 125–128.
- McDowall, R. M. 2008. "Why Are so Many Boreal Freshwater Fishes Anadromous? Confronting 'Conventional Wisdom'." *Fish and Fisheries* 9, no. 2: 208–213. <https://doi.org/10.1111/j.1467-2979.2008.00271.x>.
- Muste, M., D. Kim, and V. Merwade. 2012. "Modern Digital Instruments and Techniques for Hydrodynamic and Morphologic Characterization of River Channels." *Gravel-Bed Rivers: Processes, Tools, Environments*, edited by M. Church, P. M. Biron, and A. G. Roy, 315–341. <https://doi.org/10.1002/9781119952497.CH24>.
- Negro, G., M. Carolli, A. Andreoli, et al. 2022. Transferability of Mesohabitat Suitability Criteria in Northern Italy. Proceedings of the IAHR World Congress, 1416–1423. <https://doi.org/10.3850/IAHR-39WC2521716X20221044>.
- Negro, G., S. Fenoglio, E. Quaranta, C. Comoglio, I. Garzia, and P. Vezza. 2021. "Habitat Preferences of Italian Freshwater Fish: A Systematic Review of Data Availability for Applications of the MesoHABSIM Model." *Frontiers in Environmental Science* 9: 305. <https://doi.org/10.3389/fenvs.2021.634737>.
- Negro, G., A. Marino, S. Forte, et al. 2023. "Ecological Notes on an Endemic Freshwater Lamprey, *Lampetra zanandreae* (Vladykov, 1955)." *European Zoological Journal* 90, no. 2: 556–567. <https://doi.org/10.1080/24750263.2023.2226680>.
- Nicholas, A. P. 2003. "Investigation of Spatially Distributed Braided River Flows Using a Two-Dimensional Hydraulic Model." *Earth Surface Processes and Landforms* 28, no. 6: 655–674. <https://doi.org/10.1002/esp.491>.
- Pankhurst, N. W., and P. L. Munday. 2011. "Effects of Climate Change on Fish Reproduction and Early Life History Stages." *Marine and Freshwater Research* 62, no. 9: 1015–1026. <https://doi.org/10.1071/MF10269>.
- Parasiewicz, P. 2001. "MesoHABSIM: A Concept for Application of Instream Flow Models in River Restoration Planning." *Fisheries* 26, no. 9: 6–13. [https://doi.org/10.1577/1548-8446\(2001\)026<0006:m>2.0.co;2](https://doi.org/10.1577/1548-8446(2001)026<0006:m>2.0.co;2).
- Parasiewicz, P. 2007. "The Mesohabsim Model Revisited." *River Research and Applications* 23, no. 8: 893–903. <https://doi.org/10.1002/rra.1045>.
- Parasiewicz, P., J. N. Rogers, P. Vezza, et al. 2013. "Applications of the MesoHABSIM Simulation Model." In *Ecohydraulics*, edited by I. Maddock, A. Harby, P. Kemp, and P. Wood, 109–124. John Wiley & Sons, Ltd. <https://doi.org/10.1002/9781118526576.ch6>.
- Parasiewicz, P., K. Ryan, P. Vezza, C. Comoglio, T. Ballestero, and J. N. Rogers. 2013. "Use of Quantitative Habitat Models for Establishing Performance Metrics in River Restoration Planning." *Ecohydrology* 6, no. 4: 668–678. <https://doi.org/10.1002/eco.1350>.
- Pasternack, G. B. 2011. *2D Modeling and Ecohydraulic Analysis*. University of California at Davis.
- Pasternack, G. B., C. L. Wang, and J. E. Merz. 2004. "Application of a 2D Hydrodynamic Model to Design of Reach-Scale Spawning Gravel Replenishment on the Mokelumne River, California." *River Research and Applications* 20, no. 2: 205–225. <https://doi.org/10.1002/rra.748>.
- Paumier, A., H. Drouineau, S. Boutry, N. Sillero, and P. Lambert. 2020. "Assessing the Relative Importance of Temperature, Discharge, and Day Length on the Reproduction of an Anadromous Fish (*Alosa alosa*)." *Freshwater Biology* 65, no. 2: 253–263. <https://doi.org/10.1111/fwb.13418>.
- Pinna, B., A. Laini, G. Negro, G. Burgazzi, P. Viaroli, and P. Vezza. 2024. "Physical Habitat Modeling for River Macroinvertebrate Communities." *Journal of Environmental Management* 358: 120919. <https://doi.org/10.1016/j.jenvman.2024.120919>.
- Poff, N. L., J. D. Allan, M. B. Bain, et al. 1997. "The Natural Flow Regime: A Paradigm for River Conservation and Restoration." *Bioscience* 47, no. 11: 769–784. <https://doi.org/10.2307/1313099>.
- Probst, P., M. N. Wright, and A. L. Boulesteix. 2018. "To Tune or Not to Tune the Number of Trees in Random Forest." *Journal of Machine Learning Research* 18: 1–8.
- Puig-Mengual, C. A., A. S. Woodget, R. Muñoz-Mas, and F. Martínez-Capel. 2021. "Spatial Validation of Submerged Fluvial Topographic Models by Mesohabitat Units." *International Journal of Remote Sensing* 42, no. 7: 2391–2416. <https://doi.org/10.1080/01431161.2020.1862433>.
- Qader Mirza, M. M. 2003. "The Choice of Stage-Discharge Relationship for the Ganges and Brahmaputra Rivers in Bangladesh." *Nordic Hydrology* 34, no. 4: 321–342. <https://doi.org/10.2166/nh.2003.0010>.
- Quignard, J. P., and C. L. Douchement. 1991. *Alosa fallax* Fallax (Lacépède, 1803). In the Freshwater Fishes of Europe, 2: 225–253.
- Rapti-Caputo, D., and C. Vaccaro. 2009. "Deep Alluvial Aquifer System: An Example From the Tagliamento River Hydrogeological Basin (NE Italy)." *Bollettino di Geofisica Teorica ed Applicata* 50, no. 1: 39–50.
- Rondinini, C., A. Battistoni, and C. Teofili. 2022. "Lista Rossa IUCN dei Vertebrati Italiani 2022." Comitato Italiano IUCN e Ministero Dell'Ambiente e Della Sicurezza Energetica: Roma, Italy.
- Sabatino, S. J., R. Faria, and P. B. Alexandrino. 2022. "Genetic Structure, Diversity, and Connectivity in Anadromous and Freshwater *Alosa alosa* and *A. fallax*." *Marine Biology* 169, no. 1: 1–14. <https://doi.org/10.1007/s00227-021-03970-4>.
- Schiewe, M. H. 2013. "Salmon." *Encyclopedia of Biodiversity: Second Edition* 6: 522–531. <https://doi.org/10.1016/B978-0-12-384719-5.00293-8>.
- Seliger, C., and B. Zeiringer. 2018. "River Connectivity, Habitat Fragmentation and Related Restoration Measures." In *Riverine, Ecosystem Management*, 171–186. Springer International Publishing. https://doi.org/10.1007/978-3-319-73250-3_9.
- Šmejkal, M., A. T. Souza, P. Blabolil, et al. 2018. "Nocturnal Spawning as a Way to Avoid Egg Exposure to Diurnal Predators." *Scientific Reports* 8, no. 1: 1–7. <https://doi.org/10.1038/s41598-018-33615-4>.
- Tewinkel, G. 1963. "Water Depths From Aerial Photographs." *Photogrammetric Engineering* 29, no. 6: 1421–1428.

- Tonolla, D., V. Acuña, U. Uehlinger, T. Frank, and K. Tockner. 2010. "Thermal Heterogeneity in River Floodplains." *Ecosystems* 13, no. 5: 727–740. <https://doi.org/10.1007/s10021-010-9350-5>.
- van Puijenbroek, P. J. T. M., A. D. Buijse, M. H. S. Kraak, and P. F. M. Verdonschot. 2019. "Species and River Specific Effects of River Fragmentation on European Anadromous Fish Species." *River Research and Applications* 35, no. 1: 68–77. <https://doi.org/10.1002/rra.3386>.
- Veza, P., L. Astegiano, S. Fukuda, A. Lingua, C. Comoglio, and G. Palau-Salvador. 2016. "Using Structure From Motion Techniques to Describe and Evaluate Instream Physical Habitat." Extended Abstract, 11th International Symposium on Ecohydraulics.
- Veza, P., D. Ghia, and G. Fea. 2016. "Quantitative Habitat Models for the Conservation of the Endangered European Crayfish *Austropotamobius pallipes* Complex (Astacoidea: Astacidae)." In *A Global Overview of the Conservation of Freshwater Decapod Crustaceans*, 339–358. Cham: Springer International Publishing. https://doi.org/10.1007/978-3-319-42527-6_12.
- Veza, P., R. Muñoz-Mas, F. Martínez-Capel, and A. M. Mouton. 2015. "Random Forests to Evaluate Biotic Interactions in Fish Distribution Models." *Environmental Modelling & Software* 67: 173–183. <https://doi.org/10.1016/j.envsoft.2015.01.005>.
- Veza, P., P. Parasiewicz, O. Calles, M. Spairani, and C. Comoglio. 2014. "Modelling Habitat Requirements of Bullhead (*Cottus Gobio*) in Alpine Streams." *Aquatic Sciences* 76, no. 1: 1–15. <https://doi.org/10.1007/s00027-013-0306-7>.
- Veza, P., P. Parasiewicz, M. Rosso, and C. Comoglio. 2012. "Defining Minimum Environmental Flows at Regional Scale: Application of Mesoscale Habitat Models and Catchments Classification." *River Research and Applications* 28, no. 6: 717–730. <https://doi.org/10.1002/rra.1571>.
- Veza, P., A. Zanin, and P. Parasiewicz. 2017. Manuale Tecnico-Operativo per la Modellazione e la Valutazione Dell'integrità Dell'habitat Fluviale. In ISPra-Manuali e Linee Guida 154/2017.
- Vigiak, O., A. Pistocchi, A. Aloe, et al. 2017. "Empirical Modelling of River Water Temperature in Water Scarce European Basins." In *MODSIM2017, 22nd International Congress on Modelling and Simulation*, 880–886. Modelling and Simulation Society of Australia and New Zealand.
- Williams, R. D., J. Brasington, M. Hicks, R. Measures, C. D. Rennie, and D. Vericat. 2013. "Hydraulic Validation of Two-Dimensional Simulations of Braided River Flow With Spatially Continuous aDcp Data." *Water Resources Research* 49, no. 9: 5183–5205. <https://doi.org/10.1002/wrcr.20391>.
- Willson, M. F., S. M. Gende, and B. H. Marston. 1998. "Fishes and the Forest: Expanding Perspectives on Fish-Wildlife Interactions." *Bioscience* 48, no. 6: 455–462.
- Willson, M. F., and K. C. Halupka. 1995. "Anadromous Fish as Keystone Species in Vertebrate Communities." *Conservation Biology* 9, no. 3: 489–497. <https://doi.org/10.1046/j.1523-1739.1995.09030489.x>.
- Wohl, E., B. P. Bledsoe, R. B. Jacobson, et al. 2015. "The Natural Sediment Regime in Rivers: Broadening the Foundation for Ecosystem Management." *Bioscience* 65, no. 4: 358–371. <https://doi.org/10.1093/biosci/biv002>.
- Woodget, A. S., P. E. Carbonneau, F. Visser, and I. P. Maddock. 2015. "Quantifying Submerged Fluvial Topography Using Hyperspatial Resolution UAS Imagery and Structure From Motion Photogrammetry." *Earth Surface Processes and Landforms* 40, no. 1: 47–64. <https://doi.org/10.1002/esp.3613>.
- Wootton, R. J., and C. Smith. 2014. "Reproductive Biology of Teleost Fishes." In *Reproductive Biology of Teleost Fishes*. Wiley Blackwell. <https://doi.org/10.1002/9781118891360>.
- Yi, Y., X. Cheng, Z. Yang, S. Wierprecht, S. Zhang, and Y. Wu. 2017. "Evaluating the Ecological Influence of Hydraulic Projects: A Review of Aquatic Habitat Suitability Models." *Renewable and Sustainable Energy Reviews* 68: 748–762. <https://doi.org/10.1016/j.rser.2016.09.138>.
- Yudha Partama, I. G., A. Kanno, Y. Akamatsu, R. Inui, M. Goto, and M. Sekine. 2017. "A Simple and Empirical Refraction Correction Method for UAV-Based Shallow-Water Photogrammetry." *International Journal of Scholarly and Scientific Research & Innovation* 11, no. 4: 254–261.
- Ziliani, L., and N. Surian. 2012. "Evolutionary Trajectory of Channel Morphology and Controlling Factors in a Large Gravel-Bed River." *Geomorphology* 173: 104–117. <https://doi.org/10.1016/j.geomorph.2012.06.001>.
- Ziliani, L., and N. Surian. 2016. "Reconstructing Temporal Changes and Prediction of Channel Evolution in a Large Alpine River: The Tagliamento River, Italy." *Aquatic Sciences* 78, no. 1: 83–94. <https://doi.org/10.1007/s00027-015-0431-6>.

Supporting Information

Additional supporting information can be found online in the Supporting Information section.